

Simulating rare kaon decays $K^+ \rightarrow \pi^+ \ell^+ \ell^-$ using domain wall lattice QCD with physical light quark masses

P. A. Boyle,^{1,2} F. Erben,¹ J. M. Flynn,^{3,4} V. Gülpers,¹ R. C. Hill,^{1,3}
R. Hodgson,¹ A. Jüttner,^{3,4,5} F. Ó hÓgáin,¹ A. Portelli,^{1,*} and C. T. Sachrajda³
(RBC and UKQCD Collaborations)

¹*School of Physics and Astronomy, University of Edinburgh, Edinburgh EH9 3JZ, UK*

²*Physics Department, Brookhaven National Laboratory, Upton NY 11973, USA*

³*School of Physics and Astronomy, University of Southampton, Southampton, SO17 1BJ, UK*

⁴*STAG Research Centre, University of Southampton, Southampton, SO17 1BJ, UK*

⁵*CERN, Theoretical Physics Department, Geneva, Switzerland*

(Dated: April 12, 2022)

We report the first calculation using physical light-quark masses of the electromagnetic form factor $V(z)$ describing the long-distance contributions to the $K^+ \rightarrow \pi^+ \ell^+ \ell^-$ decay amplitude. The calculation is performed on a 2+1 flavor domain wall fermion ensemble with inverse lattice spacing $a^{-1} = 1.730(4)\text{GeV}$. We implement a Glashow-Iliopoulos-Maiani cancellation by extrapolating to the physical charm-quark mass from three below-charm masses. We obtain $V(z = 0.013(2)) = -0.87(4.44)$, achieving a bound for the value. The large statistical error arises from stochastically estimated quark loops.

I. INTRODUCTION

The $K^+ \rightarrow \pi^+ \ell^+ \ell^-$ ($\ell = e, \mu$) decays are flavor-changing neutral current processes that are heavily suppressed in the standard model (SM), and are therefore expected to be sensitive to new physics. The branching ratios for these decays, taken from the latest PDG average [1], are $\text{Br}[K^+ \rightarrow \pi^+ e^+ e^-] = 3.00(9) \times 10^{-7}$ and $\text{Br}[K^+ \rightarrow \pi^+ \mu^+ \mu^-] = 9.4(6) \times 10^{-8}$. This process is dominated by a single virtual-photon exchange ($K \rightarrow \pi \gamma^*$), whose amplitude is predominantly described by long-distance, nonperturbative physics [2]. With tensions between the measurement of the R_K ratio from LHCb and from SM predictions [3] creating increased interest in lepton-flavor universality (LFU) violations, these complementary rare kaon decays could also be suitable candidates to study LFU in the kaon sector [4].

The amplitude for the $K \rightarrow \pi \gamma^*$ decay can be expressed in terms of a single electromagnetic form factor $V(z)$ defined *via* [2, 5]

$$\mathcal{A}_\mu = -i \frac{G_F}{(4\pi)^2} V(z) [q^2 (k+p)_\mu - (M_K^2 - M_\pi^2) q_\mu], \quad (1)$$

where μ is the photon polarisation index, $z = q^2/M_K^2$, $q = k - p$, and k and p indicate the momenta of the K and π respectively. From analyticity, a prediction of $V(z)$ is given by [2]

$$V(z) = a_+ + b_+ z + V^{\pi\pi}(z), \quad (2)$$

where a_+ and b_+ are free real parameters and $V^{\pi\pi}(z)$ describes the contribution from a $\pi\pi$ intermediate state (detailed in [2]) with a $\pi^+ \pi^- \rightarrow \gamma^*$ transition. The free

parameters have, until recently, only been obtained by fitting experimental data. Having previously measured the K^+ decay channel for electrons and muons at the NA48 experiment at the CERN SPS [6], the follow-up NA62 experiment made measurements of the $K^+ \rightarrow \pi^+ \mu^+ \mu^-$ decay during the 2016-2018 Run 1 [7], with prospects for further measurements during the 2021-2024 Run 2 [8]. From the NA48 data, values of $a_+ = -0.578(16)$ and $b_+ = -0.779(66)$ have been found from the electron [6], and from the available NA62, data values of $a_+ = -0.592(15)$ and $b_+ = -0.699(58)$ from the muon [7].

In parallel, the theoretical understanding of these processes is being improved. The authors of [9, 10] construct a theoretical prediction of a_+ and b_+ by considering a two-loop low energy expansion of $V(z)$ in three-flavor QCD, with a phenomenological determination of quantities that are unknown at vanishing momentum transfer. From the electron and muon they find $a_+ = -1.59(8)$ and $b_+ = -0.82(6)$. These predictions are in significant tension with the experimental data fit, although the authors acknowledge that more work is being done to estimate more accurately the $\pi\pi$ and KK contributions.

The nonperturbative *ab-initio* approach of lattice QCD is well suited to study the dominant long-distance contribution to the matrix element of the $K^+ \rightarrow \pi^+ \gamma^*$ decay. Methods with which such a lattice calculation could be performed were first proposed in [11], and additional details on how to obtain full control of ultraviolet divergences were introduced in [12]. Following these papers an exploratory lattice calculation was performed in [13], using unphysical meson masses, in order to demonstrate how the results in [11, 12] could be applied in practice.

This letter describes a lattice calculation following the same approach as [13] but which has been performed using physical light-quark masses, thereby allowing for the first time a direct comparison to experiment.

* antonin.portelli@ed.ac.uk

II. EXTRACTION OF THE DECAY AMPLITUDE

The procedure and expressions in this section are largely a summary of the approach described in detail in [13]. We wish to compute the long-distance amplitude defined as

$$\mathcal{A}_\mu(q^2) = \int d^4x \langle \pi(\mathbf{p}) | T [J_\mu(0) H_W(x)] | K(\mathbf{k}) \rangle \quad (3)$$

in Minkowski space, where q , k , and p are defined as above, J_μ is the quark electromagnetic current and H_W is a $\Delta S = 1$ effective Hamiltonian density, given by [14]

$$H_W = \frac{G_F}{\sqrt{2}} V_{us}^* V_{ud} \sum_{j=1}^2 C_j (Q_j^u - Q_j^c), \quad (4)$$

where the C_j are Wilson coefficients, and Q_1^q and Q_2^q are the current-current operators defined (up to a Fierz transformation) by [11]

$$Q_1^q = [\bar{s}\gamma_\mu (1 - \gamma_5) d][\bar{q}\gamma^\mu (1 - \gamma_5) q], \quad (5)$$

$$Q_2^q = [\bar{s}\gamma_\mu (1 - \gamma_5) q][\bar{q}\gamma^\mu (1 - \gamma_5) d], \quad (6)$$

In practice, we use only the weak operator $O_W = \sum_{j=1}^2 C_j (Q_j^u - Q_j^c)$ and the prefactor is reintroduced at a later stage. We renormalize the operators Q_i^q nonperturbatively within the RI-SMOM scheme [15] and then follow [16] to match to the $\overline{\text{MS}}$ scheme, in which the Wilson coefficients have also been computed.

A. Correlators and Contractions

The corresponding Euclidean amplitude—which is accessible to lattice QCD calculations—can be computed by considering the “unintegrated” 4pt correlator [12]

$$\Gamma_\mu^{(4)}(t_H, t_J, \mathbf{k}, \mathbf{p}) = \int d^3\mathbf{x} \int d^3\mathbf{y} e^{-i\mathbf{q}\cdot\mathbf{x}} \langle \phi_\pi(t_\pi, \mathbf{p}) T [J_\mu(t_J, \mathbf{x}) O_W(t_H, \mathbf{y})] \phi_K^\dagger(t_K, \mathbf{k}) \rangle, \quad (7)$$

where $\phi_P^\dagger(t, \mathbf{k})$ is the creation operator for a pseudoscalar meson P at time t with momentum \mathbf{k} . To obtain the decay amplitude we take the integrated 4pt correlator [12]

$$I_\mu(T_a, T_b, \mathbf{k}, \mathbf{p}) = e^{-(E_\pi(\mathbf{p}) - E_K(\mathbf{k}))t_J} \times \int_{t_J - T_a}^{t_J + T_b} dt_H \tilde{\Gamma}_\mu^{(4)}(t_H, t_J, \mathbf{k}, \mathbf{p}), \quad (8)$$

in the limit $T_a, T_b \rightarrow \infty$. The exponential factor translates the decay to $t_J = 0$, allowing us to omit any t_J dependence in further expressions. Here $\tilde{\Gamma}_\mu^{(4)}$ is the “reduced” correlator, where we have divided out source/sink

factors and normalization contributions that are not included in the final amplitude, i.e.

$$\tilde{\Gamma}_\mu^{(4)} = \frac{\Gamma_\mu^{(4)}}{Z_{\pi K}}, \quad Z_{\pi K} = \frac{Z_\pi Z_K^\dagger L^3}{4E_\pi(\mathbf{p}) E_K(\mathbf{k})} e^{-t_\pi E_\pi(\mathbf{p}) + t_K E_K(\mathbf{k})}, \quad (9)$$

where L^3 is the spatial volume, $Z_\pi = \langle 0 | \phi_\pi(\mathbf{p}) | \pi(\mathbf{p}) \rangle$, $Z_K^\dagger = \langle K(\mathbf{k}) | \phi_K^\dagger(\mathbf{k}) | 0 \rangle$, and $E_K(\mathbf{k})$ and $E_\pi(\mathbf{p})$ are the initial-state kaon and final-state pion energies, respectively.

The spectral decomposition of Eq. (7) has been discussed in detail in [13], in particular describing the presence of intermediate one-, two-, and three-pion states between the J_μ and O_W operators. As these states can have energies $E < E_K(\mathbf{k})$ they introduce exponentially growing contributions that cause the integral to diverge with increasing T_a . These contributions do not contribute to the Minkowski decay width [12] and must be removed in order to extract the amplitude

$$\mathcal{A}_\mu(q^2) = \lim_{T_a, T_b \rightarrow \infty} \tilde{I}_\mu(T_a, T_b, \mathbf{k}, \mathbf{p}), \quad (10)$$

where \tilde{I}_μ is the integrated 4pt correlator after the exponential contributions have been subtracted. This amplitude can then be related to the Minkowski amplitude by reintroducing the previously dropped prefactor, giving $\mathcal{A}_\mu(q^2) = -iG_F V_{us}^* V_{ud} A_\mu(q^2) / \sqrt{2}$. The methods used to remove the intermediate states follow the same steps as in [13], and are outlined in Section II B.

The four classes of diagrams—Connected (C), Wing (W), Saucer (S), and Eye (E)—that contribute to the integrated correlator are represented schematically in the supplementary material. The current can be inserted on all four quark propagators in each class of diagram, in addition to a quark-disconnected self-contraction. Diagrams of these five current insertions for the C class are also shown in the supplementary material. The 20 resulting diagrams need to be computed in order to evaluate Eq. (7).

When working on the lattice there are potentially quadratically divergent contributions that come about as the operators J_μ and H_W approach each other when the current is inserted on the loop of the S and E diagrams [11, 12]. As we perform our calculation with conserved electromagnetic currents the degree of divergence is reduced to, at most, a logarithmic divergence [17] as a consequence of U(1) gauge invariance and the resulting Ward-Takahashi identity. The remaining logarithmic divergence is removed through the Glashow-Iliopoulos-Maiani (GIM) mechanism [18], implemented here through the inclusion of a valence charm quark in the lattice calculation.

B. Intermediate states

The contribution of the single-pion intermediate state can be removed by either of the two methods discussed

in [13]. The first of these (method 1) reconstructs the single-pion state using 2pt and 3pt correlators to subtract its contribution explicitly. The relevant amplitude can be extracted with this method in several ways, including a direct fit of A_μ and the intermediate state, the reconstruction of the intermediate states using fits to 2pt and 3pt correlators, a zero-momentum-transfer approximation and an SU(3)-symmetric-limit approximation, all of which are discussed in detail in [13].

The second method proposed in [13] (method 2) involves an additive shift to the weak Hamiltonian by the scalar density $\bar{s}d$ [19]

$$O'_W = O_W - c_s \bar{s}d, \quad (11)$$

where the constant parameter c_s is chosen such that

$$\langle \pi(\mathbf{k}) | O'_W | K(\mathbf{k}) \rangle = 0. \quad (12)$$

Replacing O_W with O'_W in Eq. (7) removes the contribution of the single-pion intermediate state. As the scalar density can be written in terms of the divergence of a current, the physical amplitude is invariant under such translation [12]. The two-pion contributions are expected to be insignificant until calculations reach percent-level precision and the three-pion states are even more suppressed [12]. As we do not compute the rare kaon decay amplitude to such a precision the two- and three-pion states are not accounted for in our studies.

III. DETAILS OF CALCULATION

This calculation is performed on a lattice ensemble generated with the Iwasaki gauge action and 2+1 flavors of Möbius domain wall fermions (DWF) [20]. The spacetime volume is $(L/a)^3 \times (T/a) = 48^3 \times 96$ and the inverse lattice spacing $a^{-1} = 1.730(4)\text{GeV}$. The fifth-dimensional extent is $L_s = 24$ and the residual mass is $am_{\text{res}} = 6.102(40) \times 10^{-4}$. The light and strange sea quark masses are $am_l = 0.00078$ and $am_s = 0.0362$ respectively, corresponding to pion and kaon masses of $M_\pi = 139.2(4)\text{MeV}$ and $M_K = 499(1)\text{MeV}$. We use 87 gauge configurations, each separated by 20 Monte Carlo time steps.

The Möbius DWF action [21] was used to simulate the sea quarks, with a rational approximation used for the strange quark. In this calculation the light valence quarks make use of the zMöbius action [22], an approximation of the Möbius action where the sign function has had its L_s dimension reduced by using complex parameters that have been matched to the original real parameters using the Remez algorithm. This gives a reduced fifth-dimensional extent $L_s = 10$, reducing the computational cost of light-quark inversions. The lowest 2000 eigenvectors of the Dirac operator were also calculated (“deflation”), allowing us to accelerate the light-quark zMöbius inversions further. We correct for the bias introduced by the zMöbius action with a technique similar to

all-mode-averaging (AMA) [23] by computing light and charm propagators also using the Möbius action on lower statistics, using the Möbius accelerated DWF (MADWF) algorithm [24] with deflated zMöbius guesses in the inner loop of the algorithm for the light and a mixed-precision solver for the charm quarks.

The GIM subtraction relies on a precise cancellation, in particular in the low modes of the light and charm actions, and it is paramount to use the same actions for those quarks. With the choice of zMöbius parameters for the light quark, the DWF theory breaks down for the physical charm-quark mass [25]. We instead perform the GIM subtractions using three unphysical charm-quark masses, chosen to be $am_{c_1} = 0.25$, $am_{c_2} = 0.30$, $am_{c_3} = 0.35$, and extrapolate the results to the physical point. The physical charm-quark mass was found to be $am_c = 0.510(1)$ by computing the three unphysical η_c -meson masses and extrapolating to the physical η_c mass.

We use Coulomb-gauge fixed wall sources for the kaon and pion. The pion and kaon sources are separated by 32 lattice units in time, with the kaon at rest at $t_K = 0$ and the pion with momentum $\mathbf{p} = \frac{2\pi}{L}(1, 0, 0)$ at $t_\pi = 32$. The electromagnetic current is inserted midway between the kaon and the pion at $t_J = 16$, so that the effects of the excited states from the interpolating operators are suppressed. We omit the disconnected diagram, since it is suppressed by SU(3) flavour symmetry and $1/N_c$ to an expected $\sim 10\%$ of the connected-diagram contribution [13]. Given the error on our final result, the disconnected contribution is negligible. Control of the error is being explored in an ongoing project.

We use the Möbius conserved lattice vector current [20] with only the time component $\mu = 0$, which is sufficient to extract the single form factor from Eq. (1).

To compute the loops in the S and E diagrams we use spin-color diluted sparse sources, similar to those used in [26], the structure of which is described in the supplemental material. We use the AMA technique [23] for our calculation of these diagrams, computing one hit of sparse noise with “exact” solver precision (10^{-8} , 10^{-10} , 10^{-12} , and 10^{-14} for the light, c_1 , c_2 , and c_3 quarks, respectively) and the same hit of sparse noise with “inexact” solver precision (10^{-4} for all quarks). We then compute an additional 9 hits of sparse noise with inexact solver precision and apply a correction computed from the difference of the reciprocal noises.

We performed all correlation function calculations using a dedicated software [27] based on the Grid [28, 29] and Hadrons [30] libraries, all three are free software under GPLv2. The raw lattice correlators used in this work are publicly available online [31].

IV. NUMERICAL RESULTS

The results for the 4pt functions for the lightest charm-quark mass is shown in Fig. 1, with the T_a dependence of the integrated correlator for a fixed T_b shown in Fig. 2.

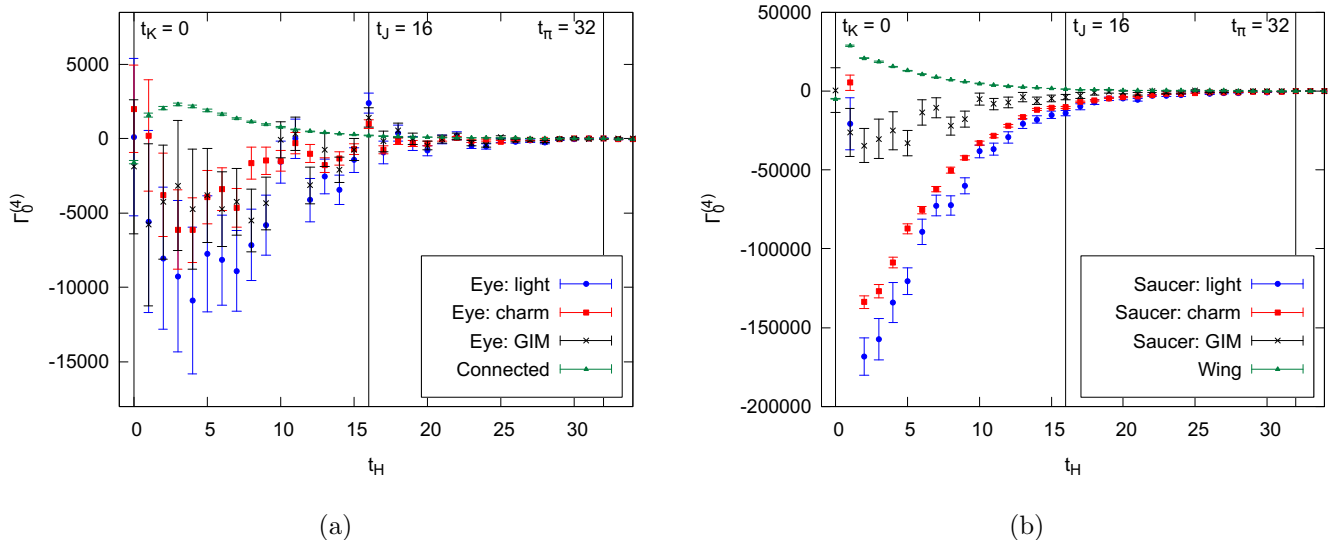


FIG. 1. The (a) Q_1 and (b) Q_2 operator contributions to the rare kaon 4-point correlator, separated into the C , W , S , and E diagrams both before and after GIM subtraction, shown for the lightest unphysical charm-quark mass $am_{c_1} = 0.25$.

The exponentially growing contributions can be seen as T_a increases and we include the result of subtracting the intermediate pion state using method 2. It is this result that we fit for A_0 , giving $A_0 = 0.00022(172)$. This result was found by performing a simultaneous fit to the corresponding 2pt functions that contribute matrix elements and energies to Eq. (9), where the 2pt functions were correlated to each other and the integrated 4pt function was correlated neither to itself nor the 2pt functions. Under these assumptions, a minimum $\chi^2/\text{dof} = 0.996$ was found; further details on the fitting procedure, including a discussion of the fit ranges which were used, are presented in the supplemental material. The error on A_0 is entirely statistical.

Table I shows the results for A_0 using the three charm-quark masses, extracted using the different methods detailed above. The results from method 2 have statistical errors that encompass the results found using method 1. As method 2 has the simplest fit structure we use it to extrapolate to the physical charm-quark mass and to compute the form factor as our final result. Fig. 3 shows the extrapolation of the method-2 results to the physical charm-quark mass, giving a value of $A_0 = 0.00035(180)$. From Eq. (1) we can relate our result to the form factor to achieve $V(z) = -0.87(4.44)$. For our choice of kinematics we have $z = 0.013(2)$; we expect the $b_+ z$ contribution to be $\sim 10^{-2}$ assuming b_+ is $\mathcal{O}(1)$, and we estimate $V^{\pi\pi}(z) = -0.00076(73)$ following [2]. We may therefore take our result for a_+ as an approximation for the intercept of the form factor.

V. CONCLUSION

We have carried out the first lattice QCD calculation of the $K^+ \rightarrow \pi^+ \ell^+ \ell^-$ decay amplitude using physi-

cal pion and kaon masses. When using physical light-quark masses, even with unphysically light charm-quark masses, the contributions in the GIM loops statistically decorrelate. This contributes to the unsatisfactory amount of noise in GIM subtraction, as can be seen in Fig. 1. Although sparse noises reduced the statistical error introduced by the single-propagator trace contribution to the Eye and Saucer diagrams, we are not able to obtain a well-resolved result for the amplitude.

The form factor that encapsulates the behavior of the long-distance amplitude of the rare kaon decay was found to be $V(0.013(2)) = -0.87(4.44)$. When this is compared to experimental results, $V^{exp}(0) \equiv a_+^{exp} = -0.578(16)$ from the electron and $a_+^{exp} = -0.592(15)$ from the muon, it can be seen that the error on our lattice result is about 8 times larger than the central value of the experimental result. However, our error is 3 times larger than the phenomenological central value obtained in [9, 10], which suggests that lattice QCD calculations will be able to provide a competitive theoretical bound

TABLE I. Fit results for A_0 for the three unphysical charm-quark masses and value found from extrapolating these to the physical point. The first four results are obtained using the various approaches to method 1, as described in Section II B, and the final result is obtained using method 2.

Analysis	m_{c_1}	m_{c_2}	m_{c_3}
<i>Method 1</i>			
Direct fit	-0.00052(208)	-0.00046(210)	-0.00040(211)
2pt/3pt recon	-0.00036(162)	-0.00024(164)	-0.00017(165)
0 mom transfer	-0.00087(165)	-0.00086(166)	-0.00086(167)
$SU(3)$ symm lim	0.00055(165)	0.00085(166)	0.00112(167)
<i>Method 2</i>			
c_s shift	0.00022(172)	0.00024(173)	0.00027(174)

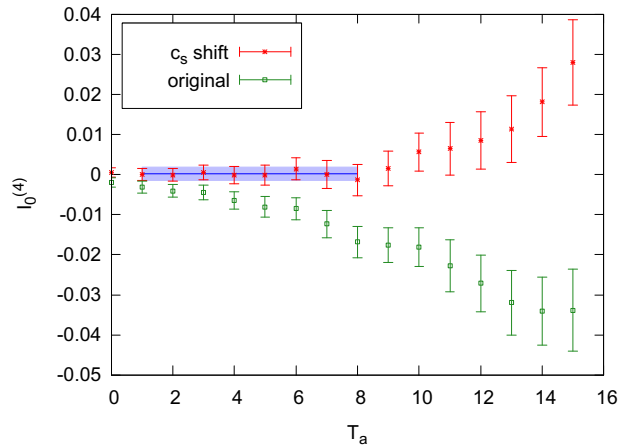


FIG. 2. The $am_{c1} = 0.25$ integrated 4pt rare kaon correlator shown for $I_0(T_a, T_b = 8, \mathbf{k}, \mathbf{p})$ (cf. Eq. (8)) to demonstrate the T_a dependence. The single-pion exponential growth has been removed using method 2. The fit to the plateau is shown in blue and gives a value of $A_0 = 0.00022(172)$.

on a_+ in the coming years.

Square-root scaling of the error tells us that obtaining an error that is of the same order as the experimental central value naively looks computationally unfeasible at this time. We would like to stress that since the noise emerges mainly from the lack of correlation in the GIM subtraction, the error obtained here has the potential to be reduced beyond square-root scaling by optimising the stochastic estimator used for the up-charm loops. Any improvements that can be made to the calculation of single-propagator traces will be crucial for the study of the decay process we are interested in. Such problems have common elements with similar challenges in computing quark-disconnected diagrams, for example as discussed in [32].

Further improvements to the analysis may come from integrating over the current insertion time t_J , as well as the weak-Hamiltonian time t_H . Though this will not tackle the dominant source of noise for this decay, its use may help to reduce the number of inversions needed to obtain the relevant 4-point functions.

Finally, it might also be possible to work in 3-flavor QCD, foregoing the calculation of the charm-quark loop [33], further reducing computational costs. This would require a new renormalization procedure which would be analogous to that of the $K \rightarrow \pi \nu \bar{\nu}$ study that was performed by the RBC-UKQCD collaborations previously [34, 35].

In conclusion, despite obtaining a first physical result

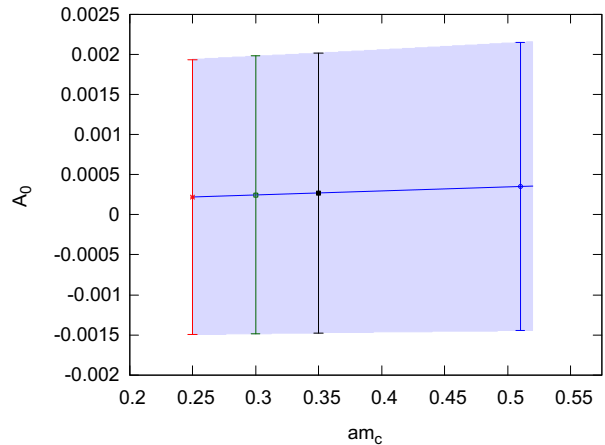


FIG. 3. The extrapolation of the A_0 results found using method 2 to the physical charm-quark mass. The linear fit and extrapolated result are shown in blue, giving a result of $A_0 = 0.00035(180)$.

with a large uncertainty, we believe that optimisation of the methodology, combined with the increased capabilities of future computers, should allow for a competitive prediction of the $K^+ \rightarrow \pi^+ \ell^+ \ell^-$ amplitude within the next years.

ACKNOWLEDGMENTS

This work used the DiRAC Extreme Scaling service at the University of Edinburgh, operated by the Edinburgh Parallel Computing Centre on behalf of the STFC DiRAC HPC Facility (www.dirac.ac.uk). This equipment was funded by BEIS capital funding via STFC capital grant ST/R00238X/1 and STFC DiRAC Operations grant ST/R001006/1. DiRAC is part of the National e-Infrastructure. PB has been supported in part by the U.S. Department of Energy, Office of Science, Office of Nuclear Physics under the Contract No. DE-SC-0012704 (BNL). FE, VG, R Hodgson, FÓh, and AP received funding from the European Research Council (ERC) under the European Union's Horizon 2020 research and innovation program under grant agreement No 757646 and AP additionally under grant agreement No 813942. R Hill was partially supported by the DISCnet Centre for Doctoral Training (STFC grant ST/P006760/1). AP, VG, FE, and R Hill are additionally supported by UK STFC grant ST/P000630/1. AJ and JF acknowledge funding from STFC consolidated grant ST/P000711/1, and AJ from ST/T000775/1. CTS was partially supported by an Emeritus Fellowship from the Leverhulme Trust and by STFC (UK) grants ST/P000711/1 and ST/T000775/1.

[1] P. Zyla *et al.* (Particle Data Group), Review of Particle Physics, PTEP **2020**, 083C01 (2020).

[2] G. D'Ambrosio, G. Ecker, G. Isidori, and J. Portolés,

- The decays $K \rightarrow \pi\ell^+\ell^-$ beyond leading order in the chiral expansion, *Journal of High Energy Physics* **1998**, 004 (1998).
- [3] R. Aaij *et al.* (LHCb), Test of lepton universality in beauty-quark decays, arXiv:2103.11769 [hep-ex] (2021).
- [4] A. Crivellin, G. D’Ambrosio, M. Hoferichter, and L. C. Tunstall, Violation of lepton flavor and lepton flavor universality in rare kaon decays, *Physical Review D* **93**, 10.1103/physrevd.93.074038 (2016).
- [5] V. Cirigliano, G. Ecker, H. Neufeld, A. Pich, and J. Portolés, Kaon decays in the standard model, *Rev. Mod. Phys.* **84**, 399 (2012).
- [6] J. Batley *et al.*, Precise measurement of the $K^+ \rightarrow \pi^+e^+e^-$ decay, *Physics Letters B* **677**, 246 (2009).
- [7] L. Bician *et al.*, New measurement of the $K^+ \rightarrow \pi^+\mu^+\mu^-$ decay at NA62, in *Proceedings of 40th International Conference on High Energy physics — PoS(ICHEP2020)*, Vol. 390 (2021) p. 364.
- [8] C. Lazzeroni (NA62 Collaboration), *2021 NA62 Status Report to the CERN SPSC*, Status Report CERN-SPSC-2021-009 ; SPSC-SR-286 (CERN SPS, Mar. 2021).
- [9] G. D’Ambrosio, D. Greynat, and M. Knecht, On the amplitudes for the CP-conserving $K^\pm(K_S) \rightarrow \pi^\pm(\pi^0)\ell^+\ell^-$ rare decay modes, *Journal of High Energy Physics* **2019**, 10.1007/jhep02(2019)049 (2019).
- [10] G. D’Ambrosio, D. Greynat, and M. Knecht, Matching long and short distances in the form factors for $K \rightarrow \pi\ell^+\ell^-$, *Physics Letters B* **797**, 134891 (2019).
- [11] G. Isidori, G. Martinelli, and P. Turchetti, Rare kaon decays on the lattice, *Physics Letters B* **633**, 75 (2006).
- [12] N. H. Christ, X. Feng, A. Portelli, and C. T. Sachrajda, Prospects for a lattice computation of rare kaon decay amplitudes: $K \rightarrow \pi\ell^+\ell^-$ decays, *Physical Review D* **92**, 10.1103/physrevd.92.094512 (2015).
- [13] N. H. Christ, X. Feng, A. Jüttner, A. Lawson, A. Portelli, and C. T. Sachrajda (RBC and UKQCD Collaborations), First exploratory calculation of the long-distance contributions to the rare kaon decays $K \rightarrow \pi\ell^+\ell^-$, *Phys. Rev. D* **94**, 114516 (2016).
- [14] G. Buchalla, A. J. Buras, and M. E. Lautenbacher, Weak decays beyond leading logarithms, *Rev. Mod. Phys.* **68**, 1125 (1996).
- [15] C. Sturm, Y. Aoki, N. H. Christ, T. Izubuchi, C. T. C. Sachrajda, and A. Soni, Renormalization of quark bilinear operators in a momentum-subtraction scheme with a nonexceptional subtraction point, *Phys. Rev. D* **80**, 014501 (2009), arXiv:0901.2599 [hep-ph].
- [16] C. Lehner and C. Sturm, Matching factors for $\Delta S = 1$ four-quark operators in RI/SMOM schemes, *Phys. Rev. D* **84**, 014001 (2011).
- [17] G. Isidori, G. Martinelli, and P. Turchetti, Rare kaon decays on the lattice, *Phys. Lett. B* **633**, 75 (2006), arXiv:hep-lat/0506026.
- [18] S. L. Glashow, J. Iliopoulos, and L. Maiani, Weak interactions with lepton-hadron symmetry, *Phys. Rev. D* **2**, 1285 (1970).
- [19] Z. Bai, N. H. Christ, T. Izubuchi, C. T. Sachrajda, A. Soni, and J. Yu, $K_L - K_S$ mass difference from lattice qcd, *Phys. Rev. Lett.* **113**, 112003 (2014).
- [20] T. Blum *et al.* (RBC and UKQCD Collaborations), Domain wall qcd with physical quark masses, *Phys. Rev. D* **93**, 074505 (2016).
- [21] R. Brower, H. Neff, and K. Orginos, The möbius domain wall fermion algorithm, *Computer Physics Communications* **220**, 1 (2017).
- [22] G. McGlynn, Algorithmic improvements for weak coupling simulations of domain wall fermions, in *Proceedings of The 33rd International Symposium on Lattice Field Theory — PoS(LATTICE 2015)*, Vol. 251 (2016) p. 019.
- [23] T. Blum, T. Izubuchi, and E. Shintani, New class of variance-reduction techniques using lattice symmetries, *Phys. Rev. D* **88**, 094503 (2013).
- [24] H. Yin and R. D. Mawhinney, Improving DWF Simulations: the Force Gradient Integrator and the Möbius Accelerated DWF Solver, *PoS LATTICE2011*, 051 (2011), arXiv:1111.5059 [hep-lat].
- [25] P. Boyle, A. Jüttner, M. K. Marinković, F. Sanfilippo, M. Spraggs, and J. T. Tsang, An exploratory study of heavy domain wall fermions on the lattice, *Journal of High Energy Physics* **2016**, 1–24 (2016).
- [26] T. Blum, P. A. Boyle, T. Izubuchi, L. Jin, A. Jüttner, C. Lehner, K. Maltman, M. Marinkovic, A. Portelli, and M. Spraggs (RBC and UKQCD Collaborations), Calculation of the hadronic vacuum polarization disconnected contribution to the muon anomalous magnetic moment, *Phys. Rev. Lett.* **116**, 232002 (2016).
- [27] F. O. hÓgáin, F. Erben, and A. Portelli, Simulation software for the paper arXiv:2202.08795 ”Simulating rare kaon decays using domain wall lattice QCD with physical light quark masses” (2022).
- [28] P. A. Boyle, G. Cossu, A. Yamaguchi, and A. Portelli, Grid: A next generation data parallel C++ QCD library, *PoS LATTICE2015*, 023 (2016).
- [29] P. Boyle, G. Cossu, G. Filaci, C. Lehner, A. Portelli, and A. Yamaguchi, Grid: Onecode and fourapis, (2022), arXiv:2203.06777 [hep-lat].
- [30] A. Portelli, R. Abott, N. Asmussen, A. Barone, P. A. Boyle, F. Erben, N. Lachini, M. Marshall, V. Gülpers, R. C. Hill, R. Hodgson, F. Joswig, F. O. hÓgáin, and J. P. Richings, *aportelli/hadrons: Hadrons v1.3* (2022).
- [31] P. A. Boyle, F. Erben, J. M. Flynn, V. Gülpers, R. C. Hill, R. Hodgson, A. Jüttner, F. O. hÓgáin, A. Portelli, and C. T. Sachrajda, Lattice dataset for the paper arXiv:2202.08795 ”Simulating rare kaon decays using domain wall lattice QCD with physical light quark masses” (2022).
- [32] L. Giusti, T. Harris, A. Nada, and S. Schaefer, Frequency-splitting estimators of single-propagator traces, *Eur. Phys. J. C* **79**, 586 (2019), arXiv:1903.10447 [hep-lat].
- [33] A. Lawson, *Exploratory lattice QCD studies of rare kaon decays*, Ph.D. thesis, University of Southampton (2017).
- [34] N. H. Christ, X. Feng, A. Portelli, and C. T. Sachrajda, Prospects for a lattice computation of rare kaon decay amplitudes. II. $K \rightarrow \pi\nu\bar{\nu}$ decays, *Physical Review D* **93**, 10.1103/physrevd.93.114517 (2016).
- [35] Z. Bai, N. H. Christ, X. Feng, A. Lawson, A. Portelli, and C. T. Sachrajda, Exploratory Lattice QCD Study of the Rare Kaon Decay $K \rightarrow \pi\nu\bar{\nu}$, *Physical Review Letters* **118**, 10.1103/physrevlett.118.252001 (2017).
- [36] S.-J. Dong and K.-F. Liu, Stochastic estimation with z 2 noise, *Phys. Lett. B*, 130–136 (1994).
- [37] J. Foley, K. J. Juge, A. Ó Cais, M. Peardon, S. M. Ryan, and J.-I. Skullerud, Practical all-to-all propagators for lattice qcd, *Computer Physics Communications* **172**, 145–162 (2005).

**Supplementary material: Simulating rare kaon decays $K^+ \rightarrow \pi^+ \ell^+ \ell^-$
using domain wall lattice QCD with physical light quark masses**

I. SPARSE SOURCES

The spacetime distribution of a source may be treated stochastically, in order to decrease the effects of local fluctuations from the gauge fields. This is important for constructing lattice propagators of the form $S(x, x)$, which are needed to calculate a disconnected diagram or a single-propagator trace contribution to a correlation function, needed for the Eye and Saucer diagrams (Fig. 6) contributing to the rare kaon decay amplitude. To create the propagators we depend on N stochastic sources κ_i that fulfill the properties

$$\begin{aligned} \lim_{N \rightarrow \infty} \frac{1}{N} \sum_{i=1}^N \kappa_i(x) &= 0, \\ \lim_{N \rightarrow \infty} \frac{1}{N} \sum_{i=1}^N \kappa_i(x) \kappa_i^\dagger(y) &= \delta_{xy}. \end{aligned} \quad (1)$$

One appropriate choice is the Z_2 source [36], where each element is randomly chosen from

$$Z_2 \otimes Z_2 = \left\{ \frac{1}{\sqrt{2}} (\pm 1 \pm i) \right\}. \quad (2)$$

It is expected that the statistical error introduced from using stochastic sources scales as $1/\sqrt{N}$. Each stochastic source here covers the full volume but we can also create “sparse sources”, similar to those described in [26], to improve the $1/\sqrt{N}$ scaling of the statistical error. In d -dimensional spacetime we create $N = n^d$ sparse sources where

$$\kappa_{\text{sparse}}(x) = \begin{cases} \kappa_{Z_2}(x) : x_\mu \bmod n = 0, & \mu = 0, 1, 2, 3 \\ 0 : \text{otherwise} \end{cases} \quad (3)$$

for the first source and we shift in each dimension to ensure that the N sources cover the entire volume with no overlap when combined, see Fig. 4 for a $d = 2$, $n = 2$ example. When investigating rare kaon decays we use $N = 2^4 = 16$ sparse sources for each hit of a propagator, $S(x, x)$, that we compute.

A cost-benefit analysis was performed using the quantity $\frac{\Delta X}{\Delta \text{Sparse}} \sqrt{\frac{N_X}{N_{\text{Sparse}}}}$, where ΔX is the statistical error of the result from method X and the root of the number of inversions N_X tracks the computational cost of using method X . Fig. 5 shows the results of this cost-benefit analysis for the 3-point Saucer diagram with zero momentum. The loop in the diagram was computed using sparse sources, full volume sources and time-diluted all-to-all vectors [37] with 2000 low modes, with the other

propagators being computed with Coulomb-gauge fixed wall sources. This was performed on RBC/UKQCD’s $48^3 \times 96$ Möbius domain wall fermion gauge ensembles [20]. It can clearly be seen that the sparse-noise approach is the most successful.

II. FURTHER RELEVANT CORRELATORS

Before giving details on the fit parameters that were used we outline the definitions of several relevant Euclidean correlation functions.

A. 2-point correlators

Given an interpolation operator $\phi_P(t, \mathbf{p})$ for a pseudoscalar meson, P , with spacial momentum \mathbf{p} at time t , for $t \gg 0$ the 2-point function

$$\Gamma_P^{(2)}(t, \mathbf{p}) = \langle \phi_P(t, \mathbf{p}) \phi_P^\dagger(0, \mathbf{p}) \rangle \quad (4)$$

has the following behavior:

$$\Gamma_P^{(2)}(t, \mathbf{p}) = L^3 \frac{|Z_P(\mathbf{p})|^2}{2E_P(\mathbf{p})} [e^{-E_P(\mathbf{p})t} + e^{-E_P(\mathbf{p})(n_t-t)}], \quad (5)$$

where $Z_P(\mathbf{p}) = \langle 0 | \phi_P(0, \mathbf{0}) | P(\mathbf{p}) \rangle$ and $E_P(\mathbf{p})$ the meson energy $\sqrt{M_P^2 + \mathbf{p}^2}$.

We calculated the pion and kaon 2pt functions using Coulomb-gauge fixed wall sources and both Coulomb-gauge fixed wall sinks and point sinks. Although we only require the wall-wall matrix elements in order to extract the decay amplitude the point-wall 2pt functions have a cleaner signal. Thus both the wall-wall and point-wall correlators can be used in a combined fit to obtain $E_P(\mathbf{p})$ with greater accuracy. All pseudoscalar/sink combinations are calculated for $\mathbf{p} = \frac{2\pi}{L}(0, 0, 0)$ and $\mathbf{p} = \frac{2\pi}{L}(1, 0, 0)$.

B. 3-point weak Hamiltonian correlator

The weak Hamiltonian 3pt function

$$\Gamma_H^{(3)}(t_H, \mathbf{p}) = \int d^3\mathbf{x} \langle \phi_\pi(t_\pi, \mathbf{p}) H_W(t_H, \mathbf{x}) \phi_K^\dagger(0, \mathbf{p}) \rangle \quad (6)$$

has the following behavior for $0 \ll t_H \ll t_\pi$:

$$\begin{aligned} \Gamma_H^{(3)}(t_H, \mathbf{p}) &= L^3 \frac{Z_\pi(\mathbf{p}) Z_K(\mathbf{p})^\dagger \mathcal{M}_H(\mathbf{p})}{4E_\pi(\mathbf{p}) E_K(\mathbf{p})} \\ &\times e^{-E_\pi(\mathbf{p})t_\pi} e^{-[E_K(\mathbf{p}) - E_\pi(\mathbf{p})]t_H} \end{aligned} \quad (7)$$

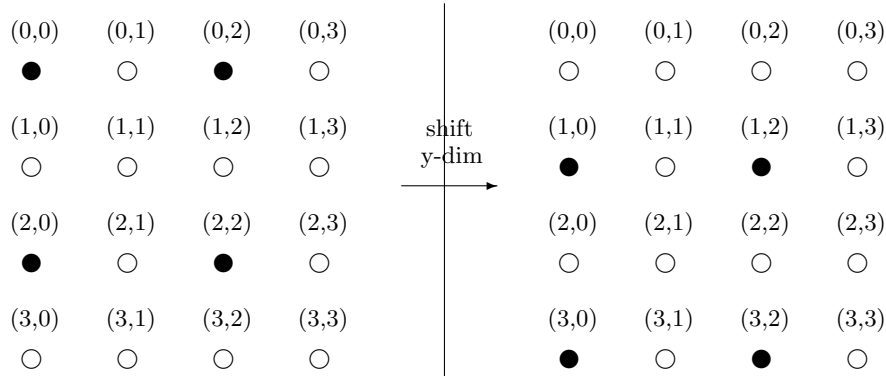


FIG. 4. An example of sparse noises for $d = 2$, $n = 2$. The filled circles represent a site with Z_2 noise, the empty circles represent a site that has been set to zero. Two further shifts are needed to cover the full volume, giving $2^2 = 4$ sparse sources.

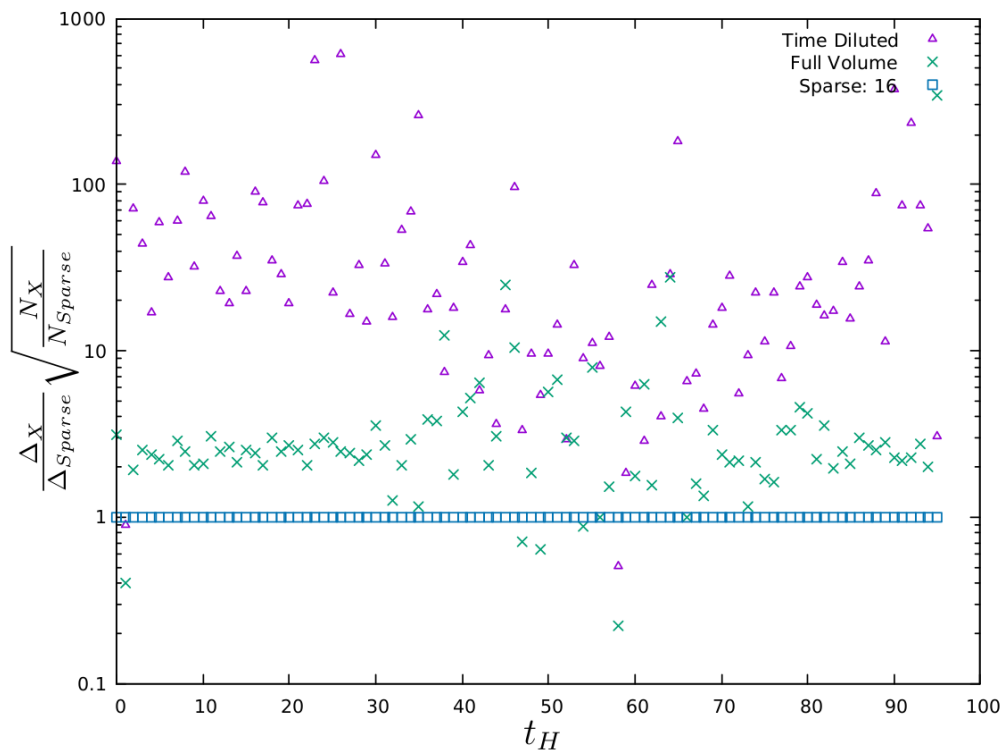


FIG. 5. The statistical error relative to that of the “Sparse: 16” noise, weighted by the cost of inversions, of the zero-momentum Saucer diagram contribution to the 3-point weak Hamiltonian correlation function, computed using different noise strategies for the single quark propagator loop.

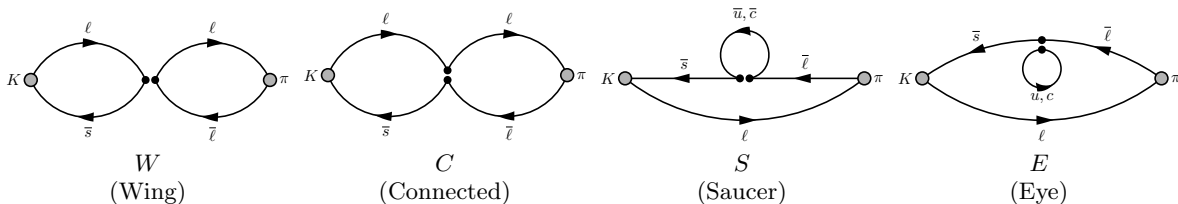


FIG. 6. The four classes of diagrams obtained after performing the Wick contractions of the charged pion and kaon interpolating operators with the H_W operator. ℓ denotes a light (u or d) quark propagator. The two black circles represent the currents in the four-quark operators $Q_{1,2}^q$ defined in the main paper. The C and E diagrams contain an insertion of Q_1^q and the W and S diagrams contain an insertion of Q_2^q .

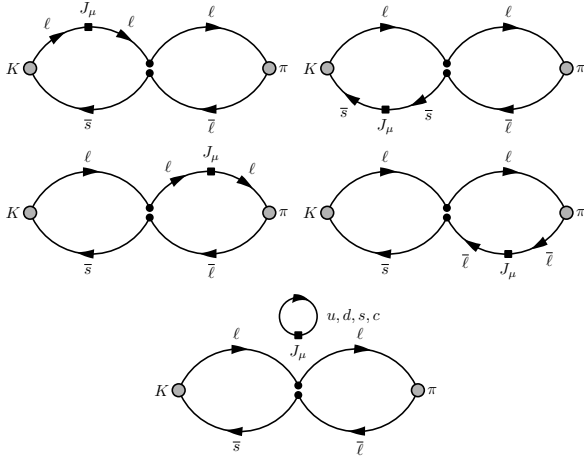


FIG. 7. The five possible current insertions for the C class of diagrams contributing to the 4pt rare kaon decay correlator. The diagrammatic conventions are the same as in Fig. 6

with $\mathcal{M}_H(\mathbf{p}) = \langle \pi(\mathbf{p}) | H_W(0) | K(\mathbf{p}) \rangle$. This correlator is calculated for both $\mathbf{p} = \frac{2\pi}{L} (0, 0, 0)$ and $\mathbf{p} = \frac{2\pi}{L} (1, 0, 0)$.

C. 3-point electromagnetic current correlator

The electromagnetic current 3pt function for a pseudoscalar meson, P ,

$$\Gamma_{J_\mu}^{(3)P}(t, t_J, \mathbf{p}, \mathbf{k}) = \int d^3\mathbf{x} e^{-i\mathbf{q}\cdot\mathbf{x}} \langle \phi_P(t, \mathbf{p}) J_\mu(t_J, \mathbf{x}) \phi_P^\dagger(0, \mathbf{k}) \rangle \quad (8)$$

has the following asymptotic behavior for $0 \ll t_J \ll t$:

$$\Gamma_{J_\mu}^{(3)P}(t, t_J, \mathbf{p}, \mathbf{k}) = L^3 \frac{Z_P(\mathbf{p}) Z_P(\mathbf{k})^\dagger \mathcal{M}_{J_\mu}^P(\mathbf{p}, \mathbf{k})}{4E_P(\mathbf{p}) E_P(\mathbf{k})} \times e^{-(t-t_J)E_P(\mathbf{p})} e^{-t_J E_P(\mathbf{k})} \quad (9)$$

where $\mathcal{M}_{J_\mu}^P(\mathbf{p}, \mathbf{k}) = \langle P(\mathbf{p}) | J_\mu(0) | P(\mathbf{k}) \rangle$. This correlator is calculated for both the pion and the kaon.

III. FIT PARAMETERS

Results of the decay amplitude are derived from global fits over all correlation functions involved in a specific fit strategy. A summary of the fit parameters for the 2pt and 3pt functions used, consistent across all fit strategies that they enter, is given in Table II. The range of T_a and T_b used in each case is given in Table III. In Fig. 8 we show the correlation matrix of the 2pt and 3pt functions, as well as slices of the integrated 4pt function, which highlights the high degree of correlation between elements of the integrated 4pt function. This correlation structure in the data makes the use of uncorrelated fits for the integrated 4pt function necessary.

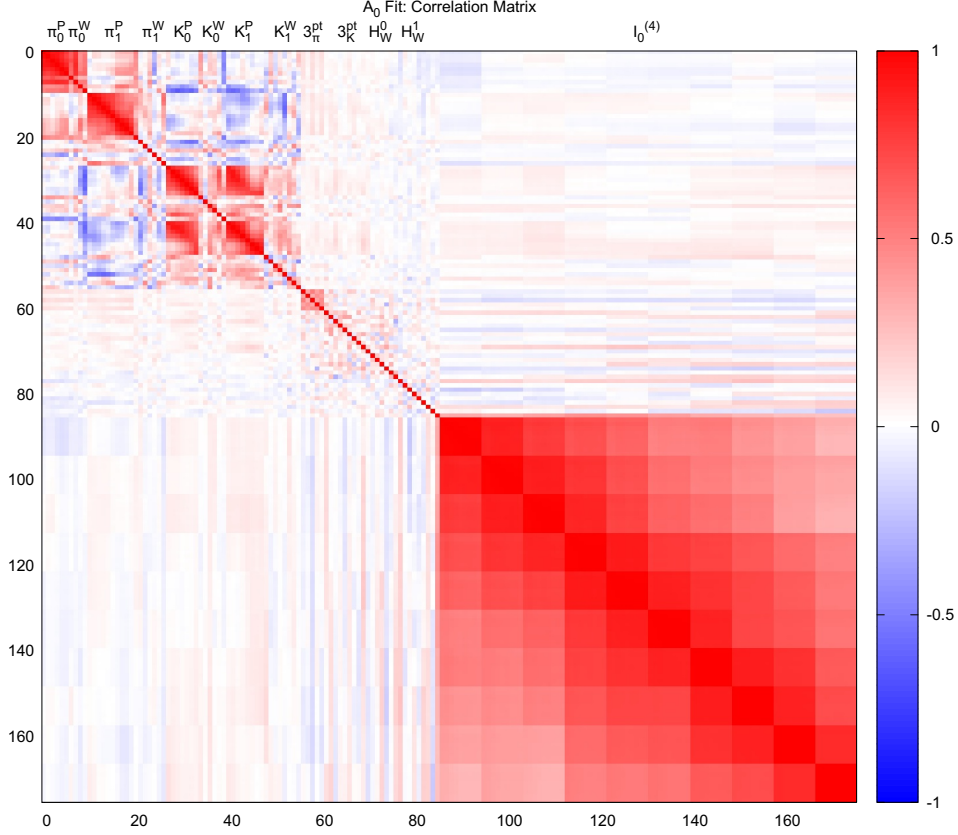


FIG. 8. The correlation matrix for the simultaneous fit used to extract A_0 . The correlators in this fit are: the 2pt pion correlator with zero momentum and a point- (π_0^P) wall-sink (π_0^W), the equivalent correlators with one unit of momentum (π_1^P , π_1^W), the same again for the kaon (K_0^P , K_0^W , K_1^P , K_1^W), the vector current inserted on the pion (3_π^{pt}) and kaon (3_K^{pt}), the 3pt weak Hamiltonian correlator with zero (H_W^0) and one unit of momentum (H_W^1), and the integrated 4pt correlator ($I_0^{(4)}$). This shows the correlation matrix for a fully correlated fit. Due to the highly correlated nature of the matrix, off-diagonal elements for the integrated 4pt function were set to zero to make the unintegrated 4pt function “uncorrelated” to the other fit variables.

TABLE II. Fit parameters for the various 2pt and 3pt correlators and methods used to extract the $K^+ \rightarrow \pi^+ \ell^+ \ell^-$ decay amplitude. With the exception of 3pt c_s each of these were correlated to each other for the relevant simultaneous fits with the integrated 4pt function. The c_s parameter was fitted separately and used as an input to the c_s shift and $c_s \times \bar{s}d$ analyses. The 3pt H_W and c_s fit parameters are the same for the three unphysical charm-quark masses. “Thinning” is the stride between data points entering the fit within the fit range.

Correlator	Momentum	Sink	t_{src}	t_i	t_f	Thinning
2pt pion	$\frac{2\pi}{L}(0, 0, 0)$	Point	32	7	18	2
2pt pion	$\frac{2\pi}{L}(0, 0, 0)$	Wall	32	13	20	2
2pt pion	$\frac{2\pi}{L}(1, 0, 0)$	Point	32	6	25	2
2pt pion	$\frac{2\pi}{L}(1, 0, 0)$	Wall	32	9	22	2
2pt kaon	$\frac{2\pi}{L}(0, 0, 0)$	Point	0	10	23	2
2pt kaon	$\frac{2\pi}{L}(0, 0, 0)$	Wall	0	9	20	2
2pt kaon	$\frac{2\pi}{L}(1, 0, 0)$	Point	0	11	26	2
2pt kaon	$\frac{2\pi}{L}(1, 0, 0)$	Wall	0	10	25	2
3pt pion	-	Wall	0	1	10	2
3pt kaon	-	Wall	0	20	35	2
3pt c_s	$\frac{2\pi}{L}(0, 0, 0)$	Wall	0	9	24	1
3pt H_W	$\frac{2\pi}{L}(0, 0, 0)$	Wall	0	17	24	2
3pt H_W	$\frac{2\pi}{L}(1, 0, 0)$	Wall	0	13	17	1

TABLE III. Fit parameters for the various methods of extracting A_0 . No thinning was performed on the integrated 4pt function data—meaning that all data points within the fit range entered the fit—which were uncorrelated when fitted simultaneously with the relevant 2pt and 3pt correlators.

Analysis	T_a min	T_a max	T_b min	T_b max
Direct fit	2	10	4	11
2pt/3pt recon	1	10	7	15
0 mom transfer	1	12	3	8
$SU(3)$ symm lim	1	10	6	13
c_s shift	1	8	5	12

Supplementary material: Simulating rare kaon decays $K^+ \rightarrow \pi^+ \ell^+ \ell^-$ using domain wall lattice QCD with physical light quark masses

P. A. Boyle,^{1,2} F. Erben,¹ J. M. Flynn,^{3,4} V. Gülpers,¹ R. C. Hill,^{1,3}
R. Hodgson,¹ A. Jüttner,^{3,4,5} F. Ó hÓgáin,¹ A. Portelli,^{1,*} and C. T. Sachrajda³
(RBC and UKQCD Collaborations)

¹*School of Physics and Astronomy, University of Edinburgh, Edinburgh EH9 3JZ, UK*

²*Physics Department, Brookhaven National Laboratory, Upton NY 11973, USA*

³*School of Physics and Astronomy, University of Southampton, Southampton, SO17 1BJ, UK*

⁴*STAG Research Centre, University of Southampton, Southampton, SO17 1BJ, UK*

⁵*CERN, Theoretical Physics Department, Geneva, Switzerland*

(Dated: April 12, 2022)

I. SPARSE SOURCES

The spacetime distribution of a source may be treated stochastically, in order to decrease the effects of local fluctuations from the gauge fields. This is important for constructing lattice propagators of the form $S(x, x)$, which are needed to calculate a disconnected diagram or a single-propagator trace contribution to a correlation function, needed for the Eye and Saucer diagrams (Fig. 3) contributing to the rare kaon decay amplitude. To create the propagators we depend on N stochastic sources κ_i that fulfill the properties

$$\begin{aligned} \lim_{N \rightarrow \infty} \frac{1}{N} \sum_{i=1}^N \kappa_i(x) &= 0, \\ \lim_{N \rightarrow \infty} \frac{1}{N} \sum_{i=1}^N \kappa_i(x) \kappa_i^\dagger(y) &= \delta_{xy}. \end{aligned} \quad (1)$$

One appropriate choice is the Z_2 source [?], where each element is randomly chosen from

$$Z_2 \otimes Z_2 = \left\{ \frac{1}{\sqrt{2}} (\pm 1 \pm i) \right\}. \quad (2)$$

It is expected that the statistical error introduced from using stochastic sources scales as $1/\sqrt{N}$. Each stochastic source here covers the full volume but we can also create “sparse sources”, similar to those described in [?], to improve the $1/\sqrt{N}$ scaling of the statistical error. In d -dimensional spacetime we create $N = n^d$ sparse sources where

$$\kappa_{\text{sparse}}(x) = \begin{cases} \kappa_{Z_2}(x) : x_\mu \bmod n = 0, & \mu = 0, 1, 2, 3 \\ 0 : \text{otherwise} \end{cases} \quad (3)$$

for the first source and we shift in each dimension to ensure that the N sources cover the entire volume with no overlap when combined, see Fig. 1 for a $d = 2$, $n = 2$

example. When investigating rare kaon decays we use $N = 2^4 = 16$ sparse sources for each hit of a propagator, $S(x, x)$, that we compute.

A cost-benefit analysis was performed using the quantity $\frac{\Delta X}{\Delta \text{Sparse}} \sqrt{\frac{N_X}{N_{\text{Sparse}}}}$, where ΔX is the statistical error of the result from method X and the root of the number of inversions N_X tracks the computational cost of using method X . Fig. 2 shows the results of this cost-benefit analysis for the 3-point Saucer diagram with zero momentum. The loop in the diagram was computed using sparse sources, full volume sources and time-diluted all-to-all vectors [?] with 2000 low modes, with the other propagators being computed with Coulomb-gauge fixed wall sources. This was performed on RBC/UKQCD’s $48^3 \times 96$ Möbius domain wall fermion gauge ensembles [?]. It can clearly be seen that the sparse-noise approach is the most successful.

II. FURTHER RELEVANT CORRELATORS

Before giving details on the fit parameters that were used we outline the definitions of several relevant Euclidean correlation functions.

A. 2-point correlators

Given an interpolation operator $\phi_P(t, \mathbf{p})$ for a pseudoscalar meson, P , with spacial momentum \mathbf{p} at time t , for $t \gg 0$ the 2-point function

$$\Gamma_P^{(2)}(t, \mathbf{p}) = \langle \phi_P(t, \mathbf{p}) \phi_P^\dagger(0, \mathbf{p}) \rangle \quad (4)$$

has the following behavior:

$$\Gamma_P^{(2)}(t, \mathbf{p}) = L^3 \frac{|Z_P(\mathbf{p})|^2}{2E_P(\mathbf{p})} [e^{-E_P(\mathbf{p})t} + e^{-E_P(\mathbf{p})(n_t-t)}], \quad (5)$$

where $Z_P(\mathbf{p}) = \langle 0 | \phi_P(0, \mathbf{0}) | P(\mathbf{p}) \rangle$ and $E_P(\mathbf{p})$ the meson energy $\sqrt{M_P^2 + \mathbf{p}^2}$.

We calculated the pion and kaon 2pt functions using Coulomb-gauge fixed wall sources and both Coulomb-gauge fixed wall sinks and point sinks. Although we only

* antonin.portelli@ed.ac.uk

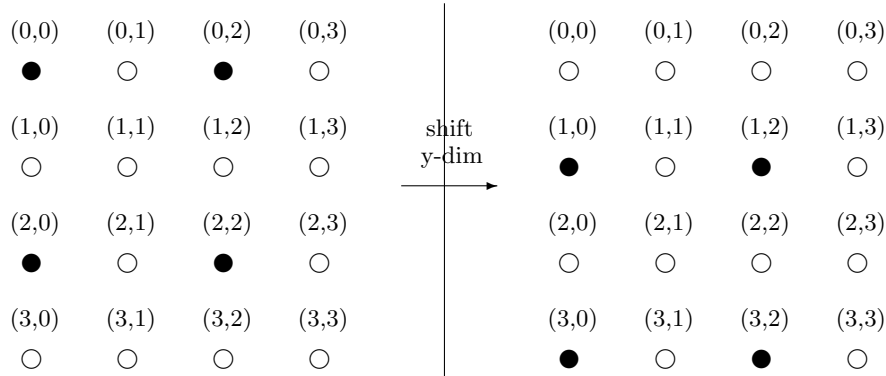


FIG. 1. An example of sparse noises for $d = 2$, $n = 2$. The filled circles represent a site with Z_2 noise, the empty circles represent a site that has been set to zero. Two further shifts are needed to cover the full volume, giving $2^2 = 4$ sparse sources.

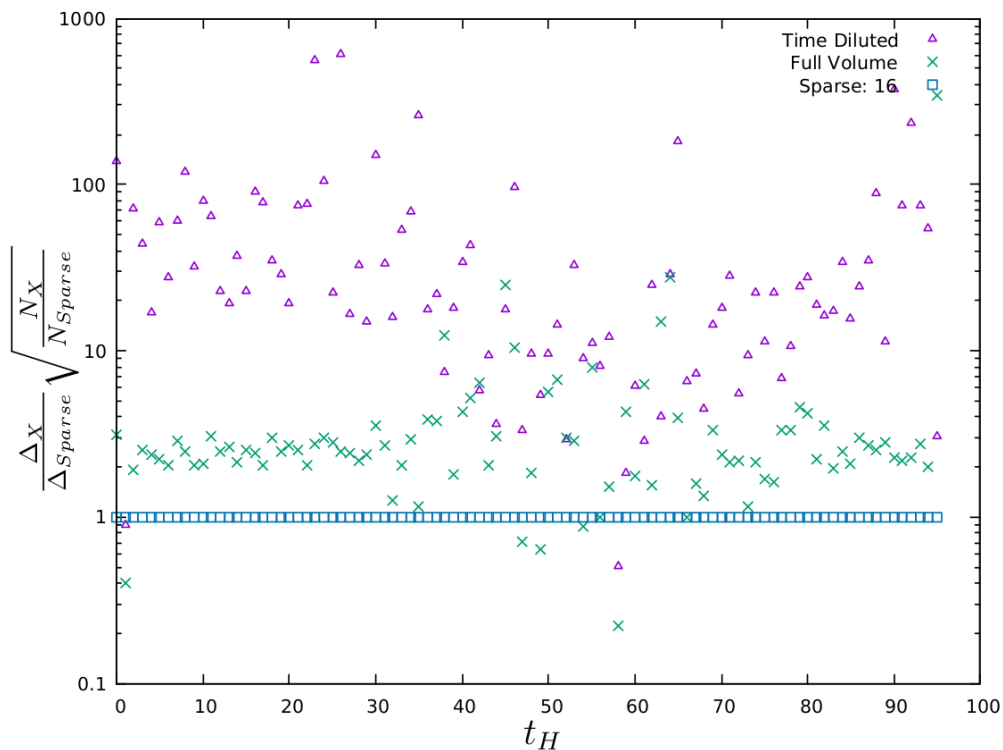


FIG. 2. The statistical error relative to that of the “Sparse: 16” noise, weighted by the cost of inversions, of the zero-momentum Saucer diagram contribution to the 3-point weak Hamiltonian correlation function, computed using different noise strategies for the single quark propagator loop.

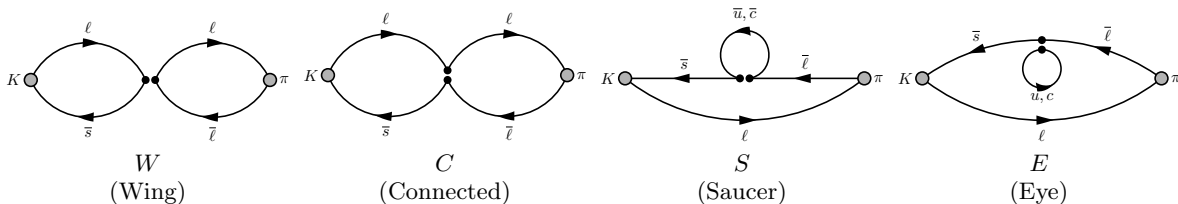


FIG. 3. The four classes of diagrams obtained after performing the Wick contractions of the charged pion and kaon interpolating operators with the H_W operator. ℓ denotes a light (u or d) quark propagator. The two black circles represent the currents in the four-quark operators $Q_{1,2}^q$ defined in the main paper. The C and E diagrams contain an insertion of Q_1^q and the W and S diagrams contain an insertion of Q_2^q .

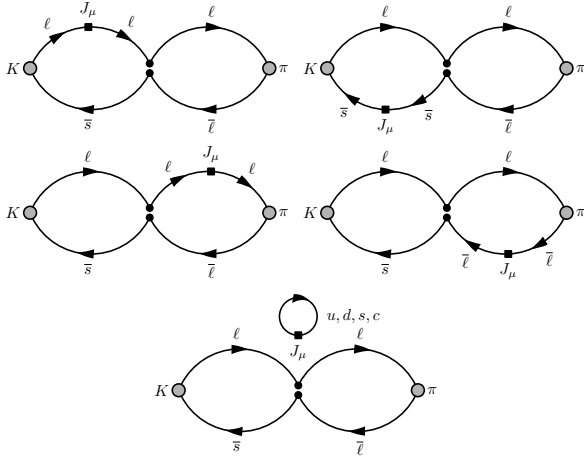


FIG. 4. The five possible current insertions for the C class of diagrams contributing to the 4pt rare kaon decay correlator. The diagrammatic conventions are the same as in Fig. 3

require the wall-wall matrix elements in order to extract the decay amplitude the point-wall 2pt functions have a cleaner signal. Thus both the wall-wall and point-wall correlators can be used in a combined fit to obtain $E_P(\mathbf{p})$ with greater accuracy. All pseudoscalar/sink combinations are calculated for $\mathbf{p} = \frac{2\pi}{L}(0, 0, 0)$ and $\mathbf{p} = \frac{2\pi}{L}(1, 0, 0)$.

B. 3-point weak Hamiltonian correlator

The weak Hamiltonian 3pt function

$$\Gamma_H^{(3)}(t_H, \mathbf{p}) = \int d^3\mathbf{x} \langle \phi_\pi(t_\pi, \mathbf{p}) H_W(t_H, \mathbf{x}) \phi_K^\dagger(0, \mathbf{p}) \rangle \quad (6)$$

has the following behavior for $0 \ll t_H \ll t_\pi$:

$$\Gamma_H^{(3)}(t_H, \mathbf{p}) = L^3 \frac{Z_\pi(\mathbf{p}) Z_K(\mathbf{p})^\dagger \mathcal{M}_H(\mathbf{p})}{4E_\pi(\mathbf{p}) E_K(\mathbf{p})} \times e^{-E_\pi(\mathbf{p})t_\pi} e^{-[E_K(\mathbf{p}) - E_\pi(\mathbf{p})]t_H} \quad (7)$$

with $\mathcal{M}_H(\mathbf{p}) = \langle \pi(\mathbf{p}) | H_W(0) | K(\mathbf{p}) \rangle$. This correlator is calculated for both $\mathbf{p} = \frac{2\pi}{L}(0, 0, 0)$ and $\mathbf{p} = \frac{2\pi}{L}(1, 0, 0)$.

C. 3-point electromagnetic current correlator

The electromagnetic current 3pt function for a pseudoscalar meson, P ,

$$\Gamma_{J_\mu}^{(3)P}(t, t_J, \mathbf{p}, \mathbf{k}) = \int d^3\mathbf{x} e^{-i\mathbf{q}\cdot\mathbf{x}} \langle \phi_P(t, \mathbf{p}) J_\mu(t_J, \mathbf{x}) \phi_P^\dagger(0, \mathbf{k}) \rangle \quad (8)$$

has the following asymptotic behavior for $0 \ll t_J \ll t$:

$$\Gamma_{J_\mu}^{(3)P}(t, t_J, \mathbf{p}, \mathbf{k}) = L^3 \frac{Z_P(\mathbf{p}) Z_P(\mathbf{k})^\dagger \mathcal{M}_{J_\mu}^P(\mathbf{p}, \mathbf{k})}{4E_P(\mathbf{p}) E_P(\mathbf{k})} \times e^{-(t-t_J)E_P(\mathbf{p})} e^{-t_J E_P(\mathbf{k})} \quad (9)$$

where $\mathcal{M}_{J_\mu}^P(\mathbf{p}, \mathbf{k}) = \langle P(\mathbf{p}) | J_\mu(0) | P(\mathbf{k}) \rangle$. This correlator is calculated for both the pion and the kaon.

III. FIT PARAMETERS

Results of the decay amplitude are derived from global fits over all correlation functions involved in a specific fit strategy. A summary of the fit parameters for the 2pt and 3pt functions used, consistent across all fit strategies that they enter, is given in Table I. The range of T_a and T_b used in each case is given in Table II. In Fig. 5 we show the correlation matrix of the 2pt and 3pt functions, as well as slices of the integrated 4pt function, which highlights the high degree of correlation between elements of the integrated 4pt function. This correlation structure in the data makes the use of uncorrelated fits for the integrated 4pt function necessary.

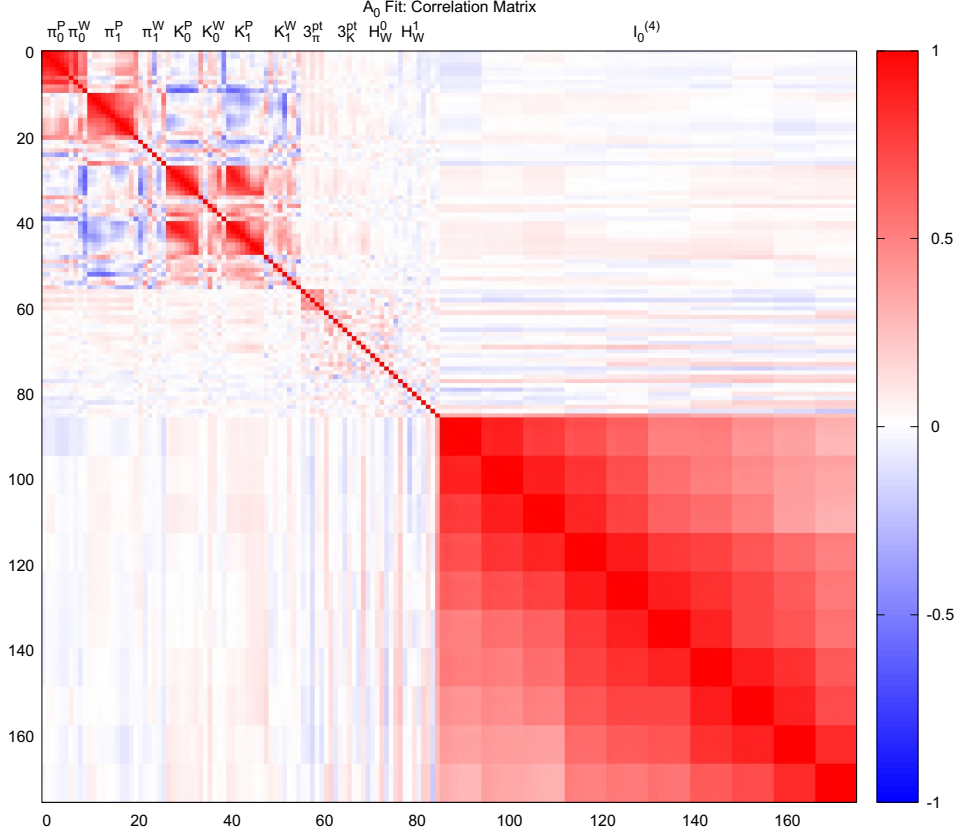


FIG. 5. The correlation matrix for the simultaneous fit used to extract A_0 . The correlators in this fit are: the 2pt pion correlator with zero momentum and a point- (π_0^P) wall-sink (π_0^W), the equivalent correlators with one unit of momentum (π_1^P , π_1^W), the same again for the kaon (K_0^P , K_0^W , K_1^P , K_1^W), the vector current inserted on the pion (3_π^{pt}) and kaon (3_K^{pt}), the 3pt weak Hamiltonian correlator with zero (H_W^0) and one unit of momentum (H_W^1), and the integrated 4pt correlator ($I_0^{(4)}$). This shows the correlation matrix for a fully correlated fit. Due to the highly correlated nature of the matrix, off-diagonal elements for the integrated 4pt function were set to zero to make the unintegrated 4pt function “uncorrelated” to the other fit variables.

TABLE I. Fit parameters for the various 2pt and 3pt correlators and methods used to extract the $K^+ \rightarrow \pi^+ \ell^+ \ell^-$ decay amplitude. With the exception of 3pt c_s each of these were correlated to each other for the relevant simultaneous fits with the integrated 4pt function. The c_s parameter was fitted separately and used as an input to the c_s shift and $c_s \times \bar{s}d$ analyses. The 3pt H_W and c_s fit parameters are the same for the three unphysical charm-quark masses. “Thinning” is the stride between data points entering the fit within the fit range.

Correlator	Momentum	Sink	t_{src}	t_i	t_f	Thinning
2pt pion	$\frac{2\pi}{L}(0, 0, 0)$	Point	32	7	18	2
2pt pion	$\frac{2\pi}{L}(0, 0, 0)$	Wall	32	13	20	2
2pt pion	$\frac{2\pi}{L}(1, 0, 0)$	Point	32	6	25	2
2pt pion	$\frac{2\pi}{L}(1, 0, 0)$	Wall	32	9	22	2
2pt kaon	$\frac{2\pi}{L}(0, 0, 0)$	Point	0	10	23	2
2pt kaon	$\frac{2\pi}{L}(0, 0, 0)$	Wall	0	9	20	2
2pt kaon	$\frac{2\pi}{L}(1, 0, 0)$	Point	0	11	26	2
2pt kaon	$\frac{2\pi}{L}(1, 0, 0)$	Wall	0	10	25	2
3pt pion	-	Wall	0	1	10	2
3pt kaon	-	Wall	0	20	35	2
3pt c_s	$\frac{2\pi}{L}(0, 0, 0)$	Wall	0	9	24	1
3pt H_W	$\frac{2\pi}{L}(0, 0, 0)$	Wall	0	17	24	2
3pt H_W	$\frac{2\pi}{L}(1, 0, 0)$	Wall	0	13	17	1

TABLE II. Fit parameters for the various methods of extracting A_0 . No thinning was performed on the integrated 4pt function data—meaning that all data points within the fit range entered the fit—which were uncorrelated when fitted simultaneously with the relevant 2pt and 3pt correlators.

Analysis	T_a min	T_a max	T_b min	T_b max
Direct fit	2	10	4	11
2pt/3pt recon	1	10	7	15
0 mom transfer	1	12	3	8
$SU(3)$ symm lim	1	10	6	13
c_s shift	1	8	5	12